Atmospheric effects on insolation in the Brazilian Amazon: Observed modification of solar radiation by clouds and smoke and derived single scattering albedo of fire aerosols

J. S. Schafer[1,2], B. N. Holben,[3] T. F. Eck[3,4], M. A. Yamasoe,[5] and P. Artaxo[5]

Received 18 January 2001; revised 20 November 2001; accepted 27 November 2001; published 11 September 2002.

[1] Five aerosol and solar flux monitoring sites were established in Brazil for the Large Scale Biosphere–Atmosphere Experiment in Amazônia (LBA) project. The first two sites were developed in the states of Rondonia and Mato Grosso in January 1999, while the others were initiated in September 1999 in Amazonas, Para, and near Brasilia (later relocated to Acre). Daily insolation [photosynthetically active radiation (PAR) and total solar] for 1999 and 9 months of 2000 was determined from flux measurements, and the daily fraction of theoretical cloud-free, background-aerosol insolation, $f_{B(day)}$, was evaluated for each site. Observed daily shortfall (MJ m^{-2} d^{-1}) of PAR insolation due to clouds and aerosols (relative to modeled values for background aerosol), and the instantaneous reductions of PAR irradiance due to high aerosol optical thickness (AOT) smoke events are presented for 1999 at Alta Floresta. The ratio of PAR flux to total solar flux (PAR fraction) was examined for all atmospheric conditions during 1999, and the observed dependence of this parameter on column water vapor and smoke AOT was quantified. No significant relationship with cloud amount (as quantified) was found. Instantaneous PAR irradiance measurements and concurrent, cloud-cleared aerosol data from collocated CIMEL sunphotometers were used with a radiative transfer model to investigate the optical properties of smoke aerosols during the burning season. In particular, the single scattering albedo (SSA) was evaluated in the PAR spectral range for $AOT_{440\ nm}$ values ranging from 0.8 to 3.0. These estimates were compared with the operational retrievals of the same parameter from algorithms developed by AERONET for CIMEL sunphotometer radiance measurements. *INDEX TERMS:* 0305 Atmospheric Composition and Structure: Aerosols and particles (0345, 4801); 0360 Atmospheric Composition and Structure: Transmission and scattering of radiation; 3309 Meteorology and Atmospheric Dynamics: Climatology (1620); 3359 Meteorology and Atmospheric Dynamics: Radiative processes

Citation: Schafer, J. S., B. N. Holben, T. F. Eck, M. A. Yamasoe, and P. Artaxo, Atmospheric effects on insolation in the Brazilian Amazon: Observed modification of solar radiation by clouds and smoke and derived single scattering albedo of fire aerosols, *J. Geophys. Res.*, *107*(D20), 8074, doi:10.1029/2001JD000428, 2002.

1. Introduction

[2] The limited number of aerosol and solar flux monitoring networks and the relative scarcity of operational sites in many large regions of the world creates a significant source of uncertainty in attempts to fully understand the global dynamics of earth-atmosphere interactions. The prevalence of these gaps in regional measurements complicates the task of effectively modeling the processes that drive our present climate, let alone forecasting accurately the future consequences of human activities. A network of five aerosol and flux monitoring sites was developed in Amazônia for this study as a part of the Large Scale Biosphere–Atmosphere Experiment in Amazônia (LBA) project to assist with filling in some of these data gaps by characterizing the aerosol and solar radiation climatology of one of the world's most vital ecosystems. The products of long-term environmental monitoring efforts such as these have applicability to improving satellite remote sensing of the earth, forest ecology and agricultural research, human health studies and, most prominently, global climate modeling projects.

[3] Atmospheric aerosols modify climate by direct absorption and scattering of solar energy and by secondary means when fine mode aerosols act as auxiliary cloud condensation nuclei (CCN), thereby decreasing average cloud droplet size and enhancing planetary albedo [*Charlson and Heintzen-*

[1]Science Systems and Applications, Inc. (SSAI), Lanham, Maryland, USA.
[2]Also at Biospheric Sciences Branch, NASA/GSFC, Greenbelt, Maryland, USA.
[3]Biospheric Sciences Branch, NASA/GSFC, Greenbelt, Maryland, USA.
[4]Also at Goddard Earth Sciences and Technology Center, University of Maryland Baltimore County, Catonsville, Maryland, USA.
[5]Departamento de Física Aplicada, Instituto de Física, Universidade de São Paulo, São Paulo, Brazil.

0148-0227/02/2001JD000428

berg, 1995; *Charlson*, 1997; *Facchini et al.*, 1999]. Additionally, absorbing aerosols may also modify climate by the semidirect effect [*Hansen et al.*, 1997] wherein heating of the aerosol layer reduces cloud cover by increasing atmospheric stability or by evaporating clouds [*Ackerman et al.*, 2000]. Highly absorbing smoke aerosols, such as are regularly produced in great quantity during the annual biomass-burning season in Amazônia, have an effect on the regional radiation budget and climate dramatically larger than that observed in even the most polluted of urban environments. Climate model designers understandably desire better quantification of the absorption properties (single scattering albedo) of tropical aerosols in the visible spectrum [*Toon*, 1995] as well as their seasonal and inter-annual variability. Also, the importance of establishing ''background'' aerosol optical thickness (AOT) levels for pristine environments (e.g. the wet season, rural Amazonian aerosol), characterizing strong regional sources (e.g., Amazonian fire centers) sufficiently for modeling purposes [*Schwartz et al.*, 1995], and better understanding the observed correlation of heavy aerosol loadings (pollution or biomass burning) with precipitation tendencies [*Rosenfeld*, 1999, 2000] are widely recognized. Many of these issues are being explored by the NASA-funded aerosol monitoring network (AERONET) whose broad reach (75+ sunphotometers worldwide) is continually extending the global record of aerosol optical properties [*Holben et al.*, 1998] (B. N. Holben, et al., An emerging ground-based aerosol climatology: Aerosol optical depth from AERONET, submitted to *Journal of Geophysical Research*, 2000). The five CIMEL sunphotometers used in this study are a subset of this network.

[4] The disparity in southern Amazônia between the wet season and dry (biomass-burning) season aerosol regimes is profound. The measurements of *Holben et al.* [1996] have shown that daily average aerosol optical thicknesses (AOT) increase by greater than an order of magnitude in southern Amazônia between the wet and dry season. Predictably, these elevated atmospheric levels of smoke aerosol produce substantial reductions in both photosynthetically active radiation (PAR) [*Eck et al.*, 1998] and total global radiation. This raises many questions about how such prolonged periods of diminished insolation (PAR, in particular), might impact the development of plant life routinely subjected to these conditions. The spectral region designated as the PAR band (400–700 nm) is of special interest as this parameter is the primary determinant of photosynthetic rates, and thus, of biomass accumulation [*Monteith and Elston*, 1993]. While the effect of reduced PAR intensity is highly species-dependent, it is known that many crops, when growing at or near their potential rate, are fully utilizing all available solar energy, and thus may suffer diminished productivity if sunlight levels were appreciably lower [*Lawlor*, 1995]. The persistent smoke-haze from the 1997 Indonesian fires was observed to suppress photosynthesis in three tree species due to high AOT values and the associated increase in atmospheric pollutant levels [*Davies and Unam*, 1999]. Further, it is believed that local forest productivity models in humid zones at least, are commonly more sensitive to solar radiation inputs than to any other climate drivers [*Aber and Freuder*, 2000]. Making a similar assessment in southern Amazônia is complicated by the tendency of plants in subequatorial, seasonally humid tropics to exhibit growth that is water-limited during parts of the driest months [*Monteith and Elston*, 1993], an effect that might supersede PAR deprivation effects. Of course, an initial step in any effort to determine the biological consequences of large PAR reductions over a long duration is to quantify the seasonal shortfall of diurnal insolation in this important spectral band that results from biomass-burning practices that consistently subject thousands of kilometers of land to a thick pall of persistent smoke-haze conditions. *Eck et al.* [1998] estimated that high smoke aerosol loadings in southern Amazônia during August–September caused reductions in PAR irradiance of 25–40% with an assumption that cloud amount was not changed by the presence of aerosols.

[5] The terrestrial remote-sensing community also stands to benefit substantially from extensive ground-based monitoring of both aerosols and solar radiation. Knowledge of AOT values representative of remote, ''background'' levels is needed for atmospheric corrections of satellite imagery, and provides higher confidence in retrieved vegetative indices (e.g., NDVI). Improved parameterization of biomass burning aerosols is essential for satellite-driven surface radiation models which are known to currently overestimate shortwave (SW) irradiance by poorly accounting for highly absorbing smoke aerosols. Large discrepancies between measured and modeled SW irradiance of 20–40 W/m2 [*Wild*, 1999] and 40–80 W/m2 [*Konzelman et al.*, 1996] have been documented in connection with prevalent savanna fires in Africa, while model overestimations of incoming solar radiation up to 44% are reported for regions of the Brazilian Amazon and Cerrado affected by biomass burning [*Pereira et al.*, 1999]. Similarly, quantification of the PAR fraction (ratio of global PAR insolation to total solar insolation) and its variability due to fluctuations of precipitable water and AOT allows for estimation of surface PAR flux from existing and future data sets (satellite-derived or surface measurements) of global shortwave radiation.

[6] Finally, numerous health-related issues are associated with the effects of elevated aerosol levels due to annual biomass burning in Amazônia. These include concerns that vectors for diseases such as malaria will have increased active periods due to sunlight reduction [*Mims et al.*, 1997], general questions about the effect of prolonged exposure to smoke (and associated tropospheric ozone) on respiratory functions, and concern that the acidity of rainwater will be increased by rainout of fire-generated aerosols, though this acidity enhancement effect has not been observed in recent studies of regions influenced by transported smoke from Indonesian fires [*Radojevik and Tan*, 2000; *Balasubramanian et al.*, 1999].

[7] In this paper we present the data and analysis of AOT, PAR and total solar fluxes for several LBA/AERONET sites in southern and central Amazônia for 1999 and nine months in 2000. In particular, the analysis focuses on the effects of water vapor, clouds and aerosols on flux and additionally on the retrieval of aerosol absorption information from synthesis of the simultaneous AOT and flux data.

2. Instrumentation and Site Descriptions

[8] Five aerosol particle and solar flux monitoring sites were established in Brazil for the LBA project (Figure 1). The first two sites were developed in the states of Rondonia

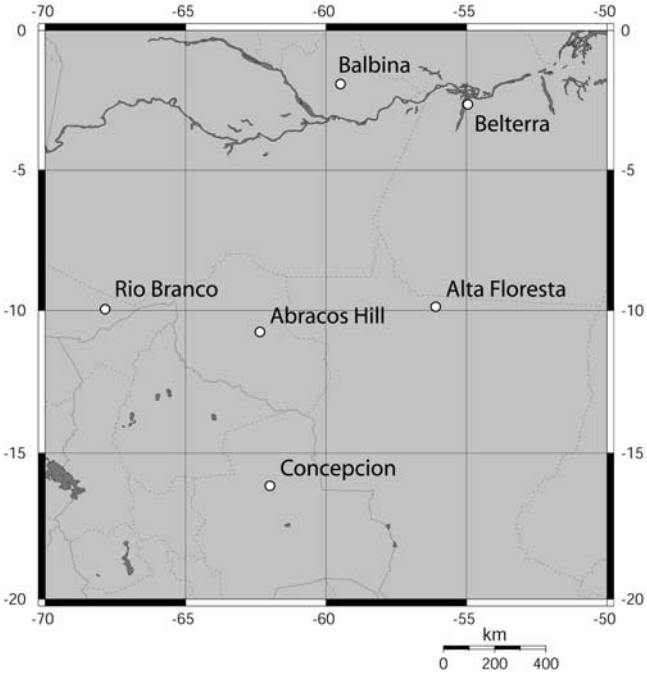

Figure 1. Site map of LBA (Alta Floresta, Abracos Hill, Balbina, Belterra, Rio Branco) and AERONET (Concepcion) aerosol and flux monitoring sites.

(Abracos Hill) and Mato Grosso (Alta Floresta) in January 1999, while the others were initiated in September 1999 in Amazonas (Balbina), Pará (Belterra) and near Brasilia. The Brasilia site was relocated to Rio Branco, Acre, in July 2000.

[9] Each site is comprised of a CIMEL sunphotometer and two flux sensors-a Skye-Probetech SKE 510 PAR (photosynthetically active radiation) Energy sensor (spectral range: 400–700 nm) and a Kipp and Zonen CM-21 pyranometer (305–2800 nm) for measuring the total solar spectrum. The flux sensors record the instantaneous irradiance at 1-minute intervals. The automatic sunphotometers (model CE-318A) were manufactured by CIMEL Electronique and their properties are discussed at length by *Holben et al.* [1998]. Each is equipped with narrow bandpass filters in the visible and near infrared with center wavelengths at 340, 380, 440, 500, 670, 870, 940, and 1020 nm. The filters are ion-assisted deposition interference filters with bandpass (FWHM) of 2 nm for the 340 nm channel, 4 nm for the 380 nm channel and 10 nm for all other channels. The CIMEL sunphotometer provides aerosol optical thickness (AOT) at each of these wavelengths, except for the 940 channel which is used to derive total column water vapor. In addition to the direct solar irradiance measurements that are made with a field of view of 1.2°, these instruments measure the sky radiance in four spectral bands (440, 670, 870, and 1020 nm) along the solar principal plane (i.e., at constant azimuth angle, with varied view zenith angles) up to 9 times a day and along the solar almucantar (i.e., at constant solar zenith angle, with varied view azimuth angles) up to 6 times a day. A preprogrammed sequence of measurements is taken by these instruments starting at an air mass of 7 in the morning and ending at an air mass of 7 in the evening. During the large air mass periods direct sun measurements are made at 0.25 air mass intervals, while at smaller air masses the interval between measurements is typically 15 min. The almucantar measurements are taken at 0.5° intervals near the Sun (within 6°), and increase from 2° to 10° intervals away from the solar position. It is these sky radiance measurements that are used to retrieve additional column aerosol properties including volume size distribution, phase function, real and imaginary component of refractive index, effective radius and single scattering albedo that are routinely computed with the AERONET inversion algorithms [*Dubovik and King*, 2000].

[10] Calibration of field sunphotometers is achieved by a transfer of calibration from reference instruments that are calibrated every 2–3 months by the Langley plot technique at Mauna Loa Observatory, Hawaii. The total uncertainty in AOT retrievals for field instruments has been estimated at 0.01–0.02, with the uncertainty increasing with shorter wavelengths [*Eck et al.*, 1998].

[11] Calibration of the PAR sensors was accomplished by using in-situ comparisons to a radiative transfer model on selected optimal days. The 6S [*Vermote et al.*, 1997] model we employed is based on the successive order of scattering method. Field days used were of minimal aerosol-loading ($AOT_{500\ nm} < 0.1$) under cloud-free conditions. Such aerosol levels are sufficiently low to render an exact knowledge of the absorption properties unimportant for computing clear-sky insolation. The factory calibration was not used as the manufacturer (Skye Probetech) states an accuracy of 5% (generally < 3%) and we desired a higher confidence in the PAR irradiance. The difference between factory calibration factor and model-derived factor for the five sites ranged from 0% to 5%, and thus was within the accuracy stated by the manufacturer.

[12] Due to additional complicating factors, such as water vapor influence, thermal equilibrium issues, and also, because of the greater degree of accuracy (2%) provided by the manufacturer (Kipp and Zonen), the factory calibrations were used for the pyranometers.

3. Analysis

[13] Daily integrated insolation (PAR and total solar) for 1999 was determined with instantaneous 1-minute sampling interval flux measurements for the 5 LBA sites. In this paper, the term insolation (PAR or total solar) will indicate the quantity of solar energy arriving at the surface in a given time interval (e.g., MJ m^{-2} d^{-1}), while irradiance will be reserved for the rate of solar energy per unit time and area (e.g., W m^{-2}) We also evaluated the fraction of theoretical cloud-free, background-aerosol insolation, $f_{B(day)}$, for each day at all sites based on modeled daily integrated values using the 6S radiative transfer model.

$$f_{B(day)} = \frac{INSOLATIONday : [AOTx; SSAx]}{INSOLATIONday : [AOT = 0.05; SSA = 0.97]}$$

The fluxes for background-aerosol conditions were estimated using an aerosol optical thickness ($AOT_{500\ nm}$) of 0.05, column water vapor of 2.0 cm and an imaginary component of refractive index of 0.003. The annual cycle of PAR and total solar daily insolation for background-aerosol conditions were modeled with the 6S radiative transfer model. Then, the ratio of each daily integrated measurement to the predicted cloudless sky, background value for the date

and site of interest was evaluated. Comparison of observed values of daily insolation on optimal, cloud-free, low-aerosol days with the modeled values for the clean atmosphere conditions show an agreement of 1–2%, and provides confidence in the calibration of the instruments.

[14] Evaluating this received fraction of cloud-free, low AOT insolation, allows for a direct comparison of the relative reductions of incident solar flux at each site due to cloud and aerosol effects without regard for latitude-dependent discrepancies (solar zenith angle). A linear interpolation algorithm was implemented to account for gaps in the 1-minute sampled flux data, based on average pre- and post gap observations. The errors associated with such interpolation were also examined by applying the algorithm to artificially introduced data gaps for days when the flux record was complete. Days of all sky conditions were used, including clear sky, partial cloud cover and overcast days. For cloudless conditions, the anticipated errors resulting from small to moderate data gaps (1–2 hours) were of negligible effect on the computed daily totals, while even for days with highly variable clouds the error for a 1 hour gap is expected to average less than 2% and not exceed 5%. For cloudy and variably cloudy conditions these errors should be random (unbiased) and thus average out on a multiday timescale. In addition, the data record reflects only days where the interpolated insolation comprised less than 10% of the total daily value.

3.1. Annual Insolation Trends

[15] The seasonal trend of the $f_{B(day)}$ weekly averages for total solar insolation (pyranometer) is quite similar at both Alta Floresta and Abracos Hill during 1999 (Figure 2a). The initial months show daily reductions that reflect the prevalent cloud cover associated with the wet season, reaching a minimum of 0.45–0.50 in February. A steady increase in the fraction of expected insolation accompanies the transition to the dry season approaching a maximum weekly average of 0.95, before the biomass burning commences. These high $f_{B(day)}$ levels are the combined result of minimal cloud cover and low, background-aerosol conditions (average $AOT_{500\ nm}$: 0.065). The rapid decline of the $f_{B(day)}$ values that subsequently begins is due exclusively to the highly elevated smoke aerosol loadings resulting from burning activity. It is noteworthy that the reductions in this 3–4 week interval (circled in the plot) are comparable to those observed in the March–May interval of the wet season due to persistent, broken cloud cover. At Alta Floresta, one week during this period of heavy smoke (average $AOT_{500\ nm} = 1.7$) experienced a prolonged reduction of daily integrated PAR insolation of approximately 35% that corresponds to a typical daily shortfall of 3–4 MJ m^{-2} in relation to background-aerosol conditions (Figure 2b). Single day reductions can exceed even these levels (Figure 3) as on 4 September 1999 at Alta Floresta ($AOT_{500\ nm} \sim 2.1$).

[16] The sites at Balbina and Belterra were installed in September of 1999 and a comparison of the first complete year of data (September 1999–September 2000) with the same interval at Alta Floresta reveals some differences (Figure 4). Balbina and Belterra are proximal to the equator (1.9 S and 2.6 S, respectively) and experience more persistent cloud cover and a less intense dry season than either Alta Floresta (9.9 S) or Abracos Hill (10.8 S) which are further south. No differences are apparent in the wetter months (January–March), with all sites exhibiting an average $f_{B(day)}$ of 0.55 to 0.6. As would be expected, a pronounced difference occurs in the dry season (preburning) period (June–July) when the $f_{B(day)}$ at the southern Amazonian sites increases to a typical value of 0.85–0.9. The equatorial sites as well see an increase in fraction of expected background insolation during this phase, but the effect is muted ($f_{B(day)}$ average: 0.65) due to the perseverance of tropical convection. The measured daily insolation reductions for 2000 at Alta Floresta and Abracos Hill track closely the pattern observed at these sites in 1999, with corresponding weekly average $f_{B(day)}$ from the 2 years generally agreeing within 10% at a given site. However, the burning season in 2000 was delayed and subdued by an unusually wet preburning phase, and this presumably created a divergence between the two years. Unfortunately, transmitter problems at both sites limited the initial months of preburning/burning season data in 2000, making difficult the direct examination of this difference.

[17] Annual median values of $f_{B(day)}$ in 1999 were 0.74 for Alta Floresta and 0.68 for Abracos Hill. By comparison, the first complete year at the equatorial sites (September 1999–September 2000) produced values that were not greatly different, with both Balbina and Belterra recording annual medians of 0.68, while Alta Floresta was 0.73 for the same interval. The median $f_{B(day)}$ at Alta Floresta was greater despite experiencing much higher daily average AOTs during the dry seasons ($AOT_{440\ nm} > 1.8$) than at Balbina or Belterra, where the daily average $AOT_{440\ nm}$ never exceeded 0.8. The most obvious distinction between the southern Amazonian and equatorial sites is in the incidence of cloud-free or minimally cloudy days. Whereas 28% of the days at Alta Floresta had a $f_{B(day)}$ value greater than 0.9 during this year interval, the percentage of days surpassing this threshold was only 8% and 12% at Belterra and Balbina, respectively.

3.2. PAR Fraction

[18] The ratio of PAR irradiance to total irradiance was examined for all atmospheric conditions. This ratio is sensitive to column water vapor, clouds and AOT. As water vapor is minimally absorbing in the PAR spectral interval, the result of increasing atmospheric water vapor is an increase in the PAR fraction, independent of other factors. Conversely, the dramatic rise in quantity of submicron radius emission particles during biomass burning episodes diminishes the transmitted PAR irradiance more strongly than the irradiance measured by the pyranometer since the resultant aerosol optical depth is much higher at the shorter (visible) wavelengths to which the PAR sensor is sensitive. Thus, increases in AOT due to smoke are always associated with a decrease in PAR fraction. The seasonal trend of day PAR fraction is shown for Alta Floresta in 1999 (Figure 5). For these purposes, the PAR fraction was simply computed as the ratio of the daily integrated values of PAR to total flux. This ratio method was used because it is intrinsically weighted more heavily during the higher solar zenith angles when the irradiance levels are greater. Taking the daily average of all the simultaneous pairs of PAR and pyranometer observations would have weighted each measurement ratio equally, even for low sun conditions that contribute negligibly to the daily insolation, and might also be influenced by the difference in

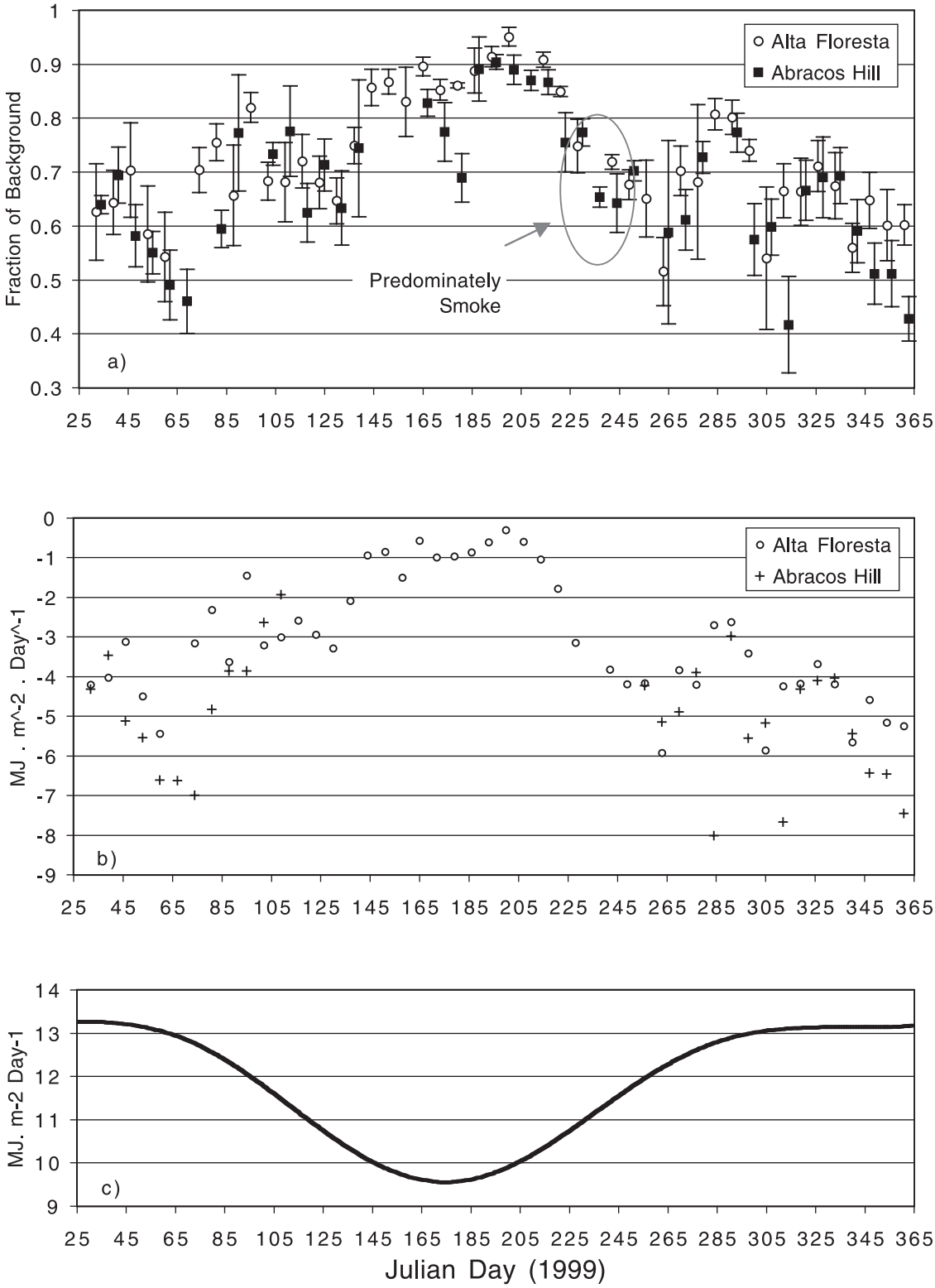

Figure 2. a) Record of the ratio of measured to modeled daily (pyranometer) insolation. The modeled insolation is for assumed cloud-free, background-aerosol conditions. Data are weekly averages of daily ratios at Alta Floresta and Abracos Hill in 1999. b) Computed shortfall in daily PAR insolation relative to that expected for cloud-free, background-aerosol conditions. Data are weekly averages of daily values (1999). c) Modeled daily PAR insolation for Alta Floresta for cloud-free, background-aerosol conditions.

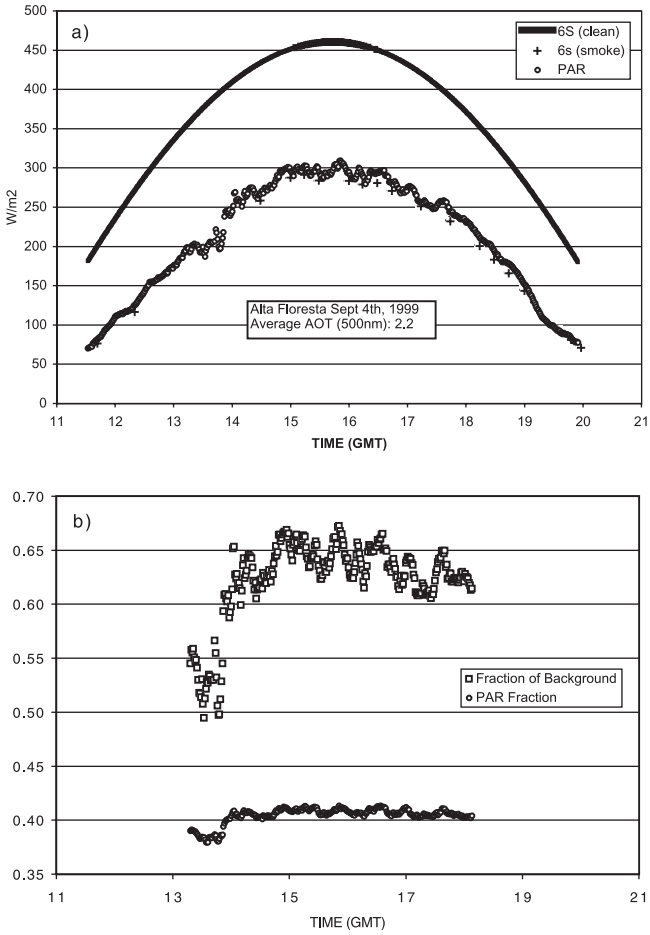

Figure 3. a) Measured PAR irradiance on 4 September 1999 at Alta Floresta exhibiting flux reduction by heavy smoke. Also shown, PAR irradiance modeled for cloud-free, background-aerosol conditions, and modeled for actual observed smoke AOT values. b) Computed fraction of modeled irradiance for background-aerosol conditions and observed instantaneous PAR fraction (ratio of PAR irradiance to pyranometer irradiance with 1-minute values).

response time of the two sensors. For the stated accuracy of the measured daily insolation (<3% for PAR, 2% for total solar insolation), the fractional uncertainty in the computed PAR fraction would be approximately 5%. This indicates that the absolute uncertainty would vary from 0.02 to 0.025 over the observed range of PAR fractions.

[19] The plot of daily average PAR fraction values for 1999 depicts a relatively consistent ratio for the wet season (January–March), though a small decline is apparent as the Amazonian dry season develops toward the end of the preburning interval (approaching day 205). This minor effect is likely a product of the diminishing column water vapor (from 5 cm to 2.5 cm). The initiation of the burning season produces dramatic decreases in PAR fraction, occasionally producing substantially lower ratios during the days of highest smoke AOT. The combination of these 2 factors effect a pronounced minimum in the August–September interval with daily PAR fractions as low as 0.39, or 0.08 less than the average for the middle of the wet season. During the preburning phase (median daily $AOT_{500\ nm}$: 0.08), the average daily PAR fraction was 0.465 ± 0.005, while the same parameter averaged 0.44 ± 0.02 for days within the burning phase (median daily $AOT_{500\ nm}$: 0.95). For comparison, the seasonal PAR fraction values when calculated as the average of all instantaneous flux measurement pairs from the year (solar zenith <40) were essentially the same as those found using ratios of daily integrals (preburning: 0.467; burning: 0.448). The lower observed column water vapor during the peak burning interval (preburning phase median: 4.82 cm; burning phase median: 3.48 cm) accounts for some of the difference in daily PAR fraction, but the major cause is the elevated smoke aerosol levels. Note that the day-to-day variability of the PAR fraction is much greater during the burning phase as well (range of daily values: 0.39–0.48) than in the preburning interval (range: 0.45–0.48), as the smoke levels fluctuate from day to day. The average PAR fraction stated here for the preburning phase is in general agreement with observed values from previous studies [*Blackburn and Proctor*, 1983; *Rao*, 1984; *Papaioannou et al.*, 1996; *Zhang et al.*, 2000], though differences in techniques and assumptions (spectral definition of PAR spectrum; day vs. hourly ratios; different sensor types) and climatic variations (column water vapor; aerosol type and optical depth) make these observations less commensurable.

3.2.1. PAR Fraction and Clouds

[20] Since these daily integral PAR fractions are based on full days of observations, they reflect various sky conditions from overcast to fully clear. The influence of clouds on PAR fraction is seen to be minor relative to that of water vapor and to AOT changes in particular, generally modifying the ratio by less than 1 percent in the annual plot. This is in contrast to simulations of cloud optical depth on PAR ratio [*Pinker and Laszlo*, 1992] which predicted a substantial increase in PAR fraction for cloudy conditions. The record of scientific literature based on empirical results is of varied opinion on this matter. Several studies have suggested a moderate or large increase in PAR fraction under cloudy conditions [*Blackburn and Proctor*, 1983; *Rodskjer*, 1983; *Rao*, 1984], while other studies indicate small or negligible increases of 2 percent or less [*Suckling et al.*, 1975; *Papaioannou et al.*, 1993, 1996].

[21] *Rao* [1984] found a significant increase in PAR fraction only for sky conditions with fractional cloud cover

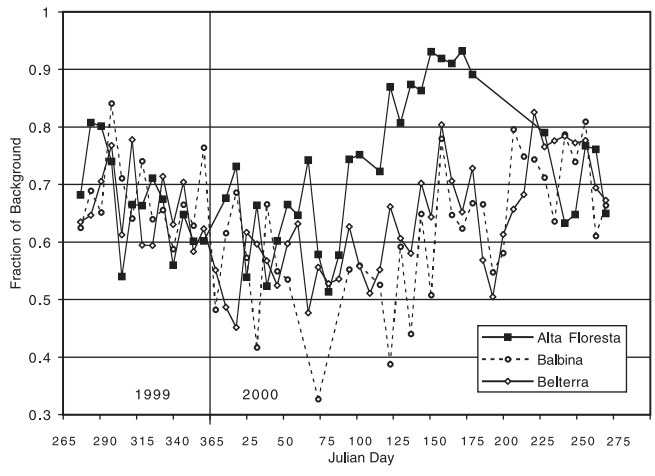

Figure 4. Record of the ratio of measured to modeled daily (pyranometer) insolation at 3 LBA sites from September 1999 to September 2000.

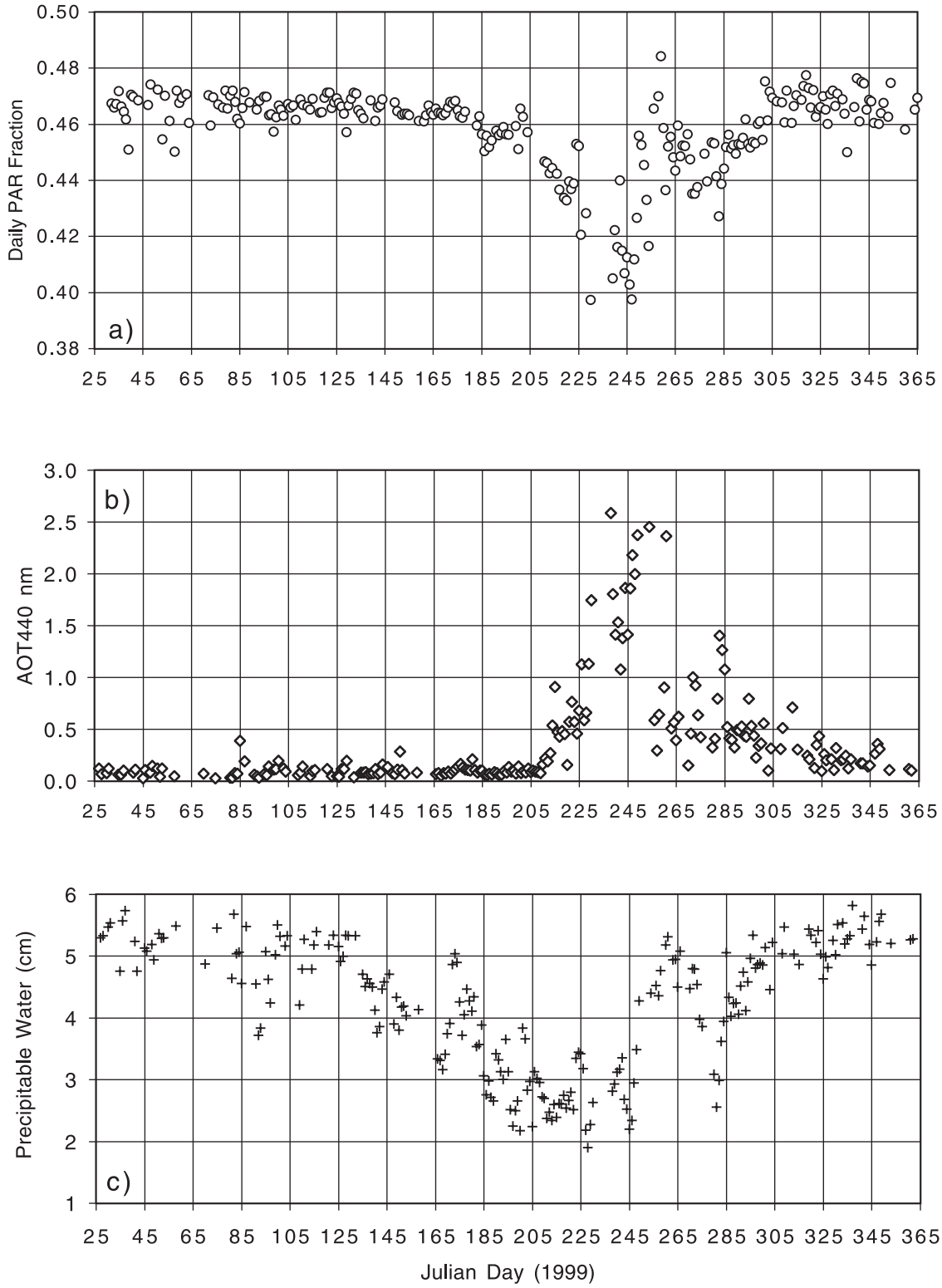

Figure 5. a) Daily PAR fraction for Alta Floresta (1999) computed as the ratio of daily PAR insolation to daily total (pyranometer) insolation. b) Daily average aerosol optical depth ($AOT_{440\ nm}$). c) Daily average precipitable water vapor (cm).

>0.85, while the observations acquired in conditions between 0.15 and 0.85 fractional coverage showed negligible difference from the 'clear' category (0.447 vs. 0.443). Various studies used different parameters to designate cloudy conditions (fractional cloud cover, sunshine duration), and the influence of water vapor or atmospheric aerosol variability on the derived PAR fraction averages was not typically quantified. Often, year or multiyear averages of PAR fraction are presented without addressing sufficiently the implications of annual variations in these

atmospheric parameters (water vapor, AOT). Consider a climate regime similar to that of the Brazilian sites: During the wet season, column water vapor levels routinely surpass 5.5 cm, while this parameter in the dry season is commonly only 2.5 cm. If one examined yearly averages of PAR fraction only, then the average for the 'cloudy' cases would be based on data disproportionately sampled from the wet season because the dry season has much less frequent cloud development. In this scenario, the effect of these higher wet season water vapor amounts alone could be falsely interpreted as an increase of PAR fraction values by clouds.

[22] To further investigate the effect of clouds on daily PAR fractions at the Abracos Hill site, the calculated $f_{B(day)}$ values were employed as an approximate indicator of cloud amount, as this parameter reflects the combined effect of cloud fraction and cloud optical thickness. The relationship between daily PAR fraction and $f_{B(day)}$ values was examined for all days prior to the burning phase (February–June 1999). Since AOT was low (<0.1 at 500 nm) for all the days considered, the dominant influence on daily PAR insolation was clouds. While the $f_{B(day)}$ parameter does not provide information about the spatial distribution of the clouds (fractional coverage), it is obvious that the minimum $f_{B(day)}$ values (as low as 0.2) designate days when received PAR was substantially diminished by optically thick clouds. Similarly, the numerous days with $f_{B(day)}$ near 1.0 were certainly days of little or no cloud cover. Even so, there is no significant trend (R^2: 0.04) of daily PAR fraction with $f_{B(day)}$. This is true as well when these same data are grouped into bins of equivalent column water vapor amounts. *Frouin and Pinker* [1995] found a similar lack of correlation between surface-measured daily PAR fraction and fractional cloud cover, although they attributed this to the use of daily integrated fluxes, stating, "at this timescale the PAR fraction variability is small".

[23] In order to explore the possibility that computing the PAR fraction as the ratio of daily integrated PAR and total solar flux masked the effect of clouds, the instantaneous PAR fraction was plotted for three narrow (5 or 10 degree) solar zenith angle bins for flux measurement pairs over the same preburning interval at Alta Floresta in 1999. The solar zenith angle ranges used were 0–10, 20–25 and 35–40, and the number of days included in each bin was dependant on the seasonal changes in solar geometry. The smallest solar zenith bin had a range of 10 degrees to increase the quantity of qualifying observations. The 0–10 degree bin represented averages from February to March 1999 at Alta Floresta, the 20–25 degree bin covered February–April, and the 35–40 degree bin spanned the full preburning (February–June) interval. The number of measurement pairs in each selected solar zenith bin, ranged from 3092 (SZ: 0–10) up to 7914 (SZ: 35–40).

[24] For each qualifying 1-minute, instantaneous PAR measurement, the ratio of the measured flux to the theoretical, clear-sky flux for background-aerosol conditions at the relevant solar zenith angle (6S modeled data) was determined, $f_{B(ins)}$. The PAR fractions were then plotted versus the corresponding $f_{B(ins)}$ values. The results for the 35–40 degree solar zenith range are shown in Figure 6a. In this case, since 1-minute flux pairs were being used, the $f_{B(ins)}$ parameter was more difficult to interpret as a measure of cloud magnitude. Large $f_{B(ins)}$ near 1.0 may demonstrate

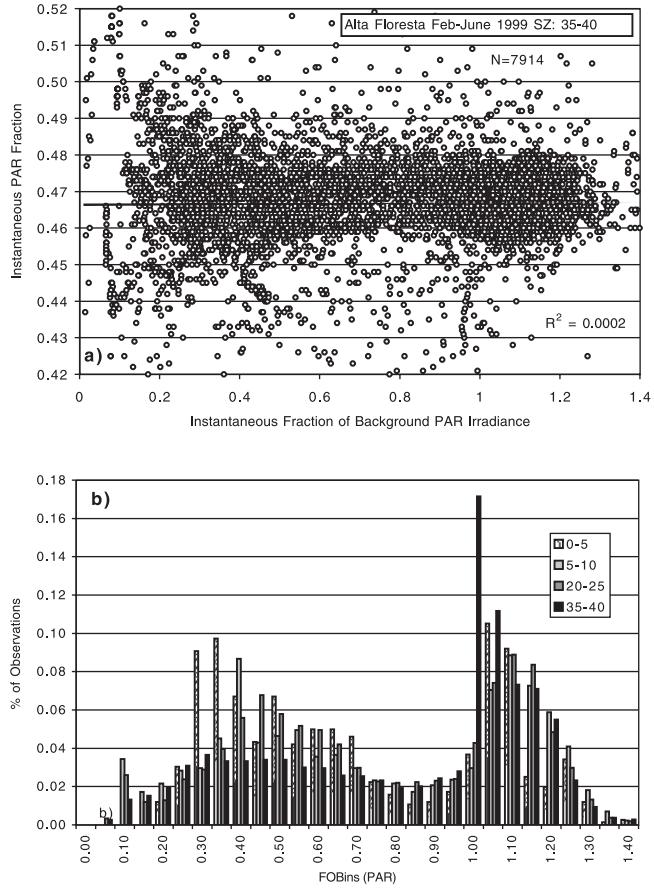

Figure 6. a) Instantaneous PAR fraction (1 minute values) versus observed fraction of modeled PAR irradiance for cloud-free background-aerosol conditions (measured PAR/modeled PAR (background)). Data represent all observations with solar zenith range between 35 and 40 degrees during the period February–June 1999 at Alta Floresta. b) Histogram of relative incidence of fraction of background ($f_{B(ins)}$) values (measured PAR irradiance/modeled PAR (background)) for four different solar zenith angle ranges from Alta Floresta during the pre-burning season in 1999.

either cloud-free conditions or enhanced PAR irradiances during broken cloud cover due to reflections from vertically developed cloud edges. This is a common effect and $f_{B(ins)}$ often reach 1.2 or more. Still, the observed low $f_{B(ins)}$ values, some lower than 0.1, clearly result from surface PAR fluxes that are strongly reduced by cloud. Despite this, there is no trend evident for any of the three solar zenith angle groups, and the linear correlation coefficients for all 3 groups are insignificant (SZ: 0–10 R^2 = 0.003; SZ: 20–25 R^2 = 0.005; SZ: 35–40 R^2 = 0.0002). The 35–40 degree plot is most relevant in this regard since it includes data from the wet season as well as numerous observations during the early dry, preburning season (i.e., sunny days). Even so, the median PAR fraction for all cases occurring in the cloudiest conditions ($f_{B(ins)}$: 0.0 to 0.1) was 0.464 which is negligibly different from the median value for the 0.9 to 1.0 $f_{B(ins)}$ range (0.466), with the only apparent effects of clouds on PAR fraction being greater variability in this parameter. This greater variability is likely due to instrumental response differences evident for 1-minute comparisons because the

response time of the PAR sensor (10 ns) is much shorter than that of the pyranometer (<5 s). This effect will average out for a full day of instantaneous PAR fraction measurements, and is negligible for daily PAR fractions computed as the ratio of daily integrated values of PAR to total insolation.

[25] An additional plot (Figure 6b) characterizes the prevalent enhancements of surface irradiance above expected clear sky values at Alta Floresta due to reflection from edges of vertically developed clouds. A histogram of calculated $f_{B(ins)}$ values for all qualifying PAR irradiance data from four 5 degree solar zenith ranges (0–5, 5–10, 20–25 and 35–40) was generated with the Alta Floresta measurements to demonstrate the fractional contribution from observations in every $f_{B(ins)}$ bin. The great number of enhanced observations is a prominent feature for every solar zenith range, indicating that at least for the tropical convective regime, conditions that produce such elevated surface flux events are persistent and that the resulting increases in PAR flux are often substantial. As mentioned above, these data reflect a range of days from 1999 that increases with solar zenith angle so that while the 0–5 range only includes data from February, the data presented for the 35–40 zenith bin extends to observations through June. This inclusion of preburning dry season data is reflected in the distinct 0.95–1.0 $f_{B(ins)}$ spike for the 35–40 plot which results from the contribution of many cloud-free observations in June. Even so, all four zenith intervals have a significant fraction of enhanced observations with a PAR irradiance increase of 10% or more observed for 19% of the measurements in the 0–5 zenith range, and 24% of the measurements in the 35–40 zenith range. The clear sky PAR flux used to determine $f_{B(ins)}$ values were calculated based on assumed background-aerosol conditions, which is in good agreement with the actual aerosol optical thickness values measured over this interval ($AOT_{500\,nm}$: 0.06 ± 0.02).

[26] A pair of selected days demonstrates the minimal effect of clouds on the PAR fraction. We considered two dates which had comparable column water vapor amounts (diurnal range: 3.7–4.3 cm), and very low daily average $AOT_{500\,nm}$ (0.07 for both). Of these, 22 May was a completely cloud-free day, while the cloud conditions on 19 May transitioned from heavily overcast to broken cumulus, yet both demonstrated a PAR fraction of 0.46–0.47 (Figure 7).

3.2.2. PAR Fraction and Water Vapor

[27] The effect of water vapor on PAR fraction was quantified at Alta Floresta for all low aerosol days ($AOT_{500\,nm} < 0.1$). Observed AOTs on these days were sufficiently low to have a negligible influence on PAR fraction variability. Daily PAR fraction was computed as above and plotted versus daily average water vapor (Figure 8a). In addition, instantaneous measurements (based on the 1-minute flux sensor observations) of this parameter were plotted against simultaneous (within ± 1 minute) water vapor measurements from the collocated CIMEL sunphotometer (Figure 8b). The solar zenith range was small for the instantaneous observations included here (SZ: 35 ± 5) to minimize variability due to changing solar geometry. These instantaneous irradiance ratios were matched only to water vapor retrievals drawn from a sunphotometer database of cloud-screened CIMEL observations [*Smirnov et al.*, 2000], although this screening algorithm only ensures that the sky near the solar position is free of clouds. Despite the difference in methods, the two derived relationships are very similar. The modeled (6S model) PAR fraction for an assumed $AOT_{500\,nm}$ of 0.1 is also shown on this plot and agrees with the observed trend within the uncertainties of the flux measurements. A dependence of the form A ln(x) + B was suggested by the model (where x is column water vapor amount in cm) and a best fit trendline of this type indicates the reduction in PAR fraction due to a 1 cm increase in precipitable water ranges from 1% to 0.5%, with the effect diminishing for higher values of column water vapor.

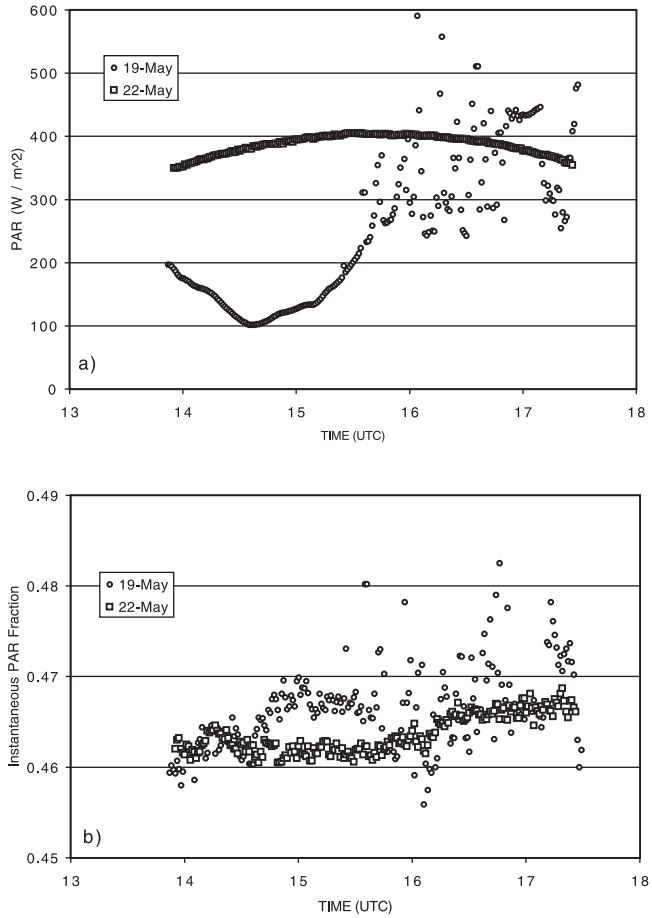

Figure 7. a) Measured PAR irradiance on 19 May and 22 May at Alta Floresta in 1999. b) Computed instantaneous PAR fraction for the same days based on 1-minute measurement pairs.

3.2.3. PAR Fraction and Smoke Aerosol

[28] To examine the substantial reduction in PAR fraction due to smoke aerosol, measurements made exclusively during smoke events were considered. Observations acquired during the season of burning activity which exhibited an Angstrom wavelength exponent greater than 1.0 and an $AOT_{500\,nm}$ of greater than 0.5, determined with simultaneous, cloud-screened AOT retrievals from the CIMEL, were considered to be associated with a smoke event. The associated precipitable water amounts were between 3 and 4 cm, typical of the dry season, and a limited range of solar zenith angles (35 ± 5) was allowed. For the qualifying measurements, the instantaneous PAR fraction was plotted versus the associated AOT determined from the CIMEL sunphotometer (Figure 9).

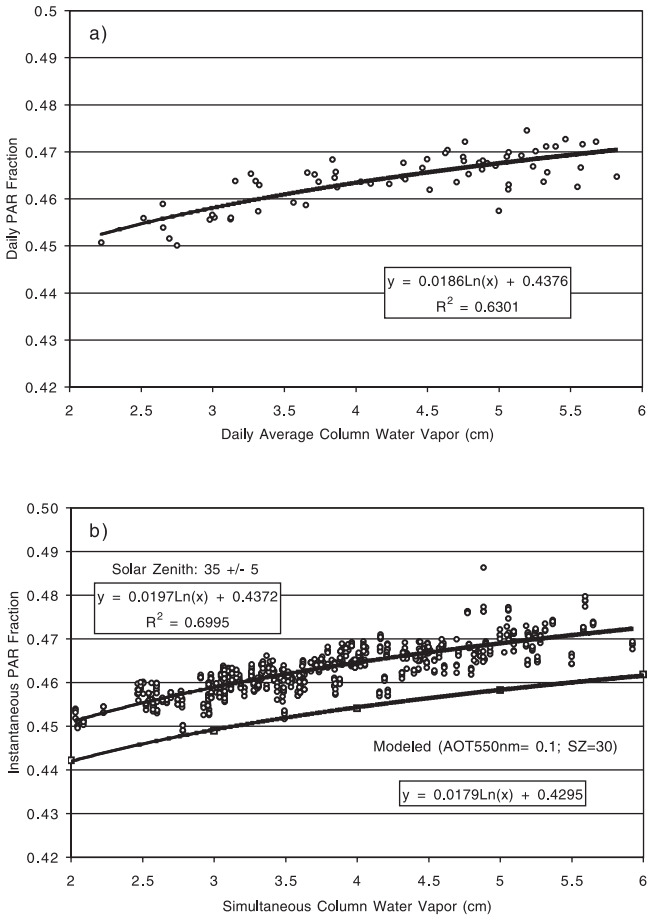

Figure 8. a) Daily PAR fraction versus daily average precipitable water (cm) for days of low aerosol optical depth (day average $AOT_{500\ nm} < 0.1$) at Alta Floresta in 1999. b) Instantaneous PAR fraction ($AOT_{500\,nm} < 0.1$) versus simultaneous precipitable water vapor measurements. Modeled PAR fraction dependence on column water vapor is also shown for an assumed $AOT_{500\,nm}$ of 0.1.

The resulting regression indicates a significant reduction in PAR fraction (0.028) for an increase in $AOT_{500\ nm}$ of 1.0. The correlation of PAR fraction with smoke AOT is very strong (0.94) and indicates a PAR fraction of 0.39 for an $AOT_{500\ nm}$ of 2.5 which is markedly lower than average, wet season PAR fraction measurements (0.47).

[29] While the influence of smoke AOT fluctuation on the PAR fraction is much more dramatic than that of precipitable water changes, this is due in part to the wider range of values of this parameter, and its greater temporal variability. Whereas column water may range annually from 2 cm to 6 cm, a factor of 3 change, the AOT observed in the wet season commonly differs by factor of 50 from that measured at the height of burning. Even within the burning season the smoke AOT may fluctuate by a factor of 5 or more within a few days, and this is evident in the variability in the PAR fraction during this period.

3.3. PAR Attenuation by Smoke Aerosols

[30] Clearly, based on examining the PAR fraction, flux in the PAR spectral region is diminished by smoke disproportionately relative to the total solar spectrum. It is of interest, then, to quantify this reduction of PAR irradiance by biomass burning in absolute energy units. In the same manner as for the instantaneous PAR fraction plots, PAR sensor measurements were matched to simultaneous, cloud-screened CIMEL observations for a limited range of solar zenith angles (25–35). For each matched observation, the PAR irradiance expected for background-aerosol conditions (background aerosol: $AOT_{500\ nm}$: 0.05) was determined with the 6S radiative model. To minimize any effect of water vapor variability, the PAR was modeled using the observed (CIMEL-derived) column water vapor to compute each expected clear sky flux, though the range of precipitable water was quite small during the burning season. For consistency, the radiative transfer code used to model these fluxes was the same one used for the in situ PAR sensor under low AOT conditions.

[31] The observed PAR irradiances were then subtracted from the modeled values to estimate the reduction in PAR (W m^{-2}) due to smoke aerosol. This procedure was applied to three Amazonian sites (1999—Alta Floresta and Abracos Hill; 1998—Concepcion) during their respective burning seasons (Figure 10a). The observed PAR reductions were quite similar at all locations, indicating an approximate loss of 86 W m^{-2} at an aerosol optical thickness of 1.0 (500 nm). The efficiency (regression slope of PAR reduction vs. AOT) of smoke attenuation was also comparable, ranging from -53 W m^{-2} to -62 W m^{-2} for a unit change of $AOT_{500\ nm}$. For comparison, the average reduction in PAR irradiance at the same site in the peak wet season interval February–April (SZ: 20–25) was -122 W m^{-2} for observations under all sky conditions. Given that the median $AOT_{500\ nm}$ during the interval of heaviest smoke is near 1.0, the typical reductions in PAR irradiance resulting from biomass burning are seen to be about 70% of the average reductions due to clouds during the middle of the wet season.

[32] These rates of PAR reduction by smoke are in good agreement with modeled PAR reductions (Figure 10b) using CIMEL-derived smoke volume size distributions selected by AOT. The best agreement with the observed data, in terms of PAR attenuation rate by smoke aerosol is for the cases with an input SSA equal to 0.95 and 0.90, which predict a PAR attenuation rate of -55 W m^{-2} and -65 W m^{-2} respectively for a unit change in $AOT_{500\ nm}$. These are reasonable single scattering albedos for the smoke of this

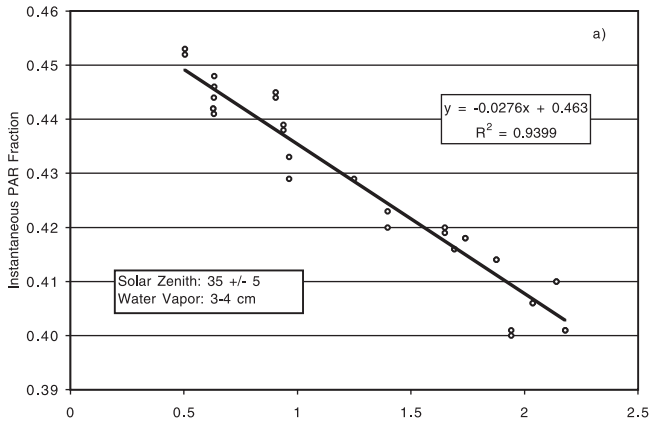

Figure 9. Instantaneous PAR fraction versus simultaneous CIMEL sunphotometer-derived AOT measurements.

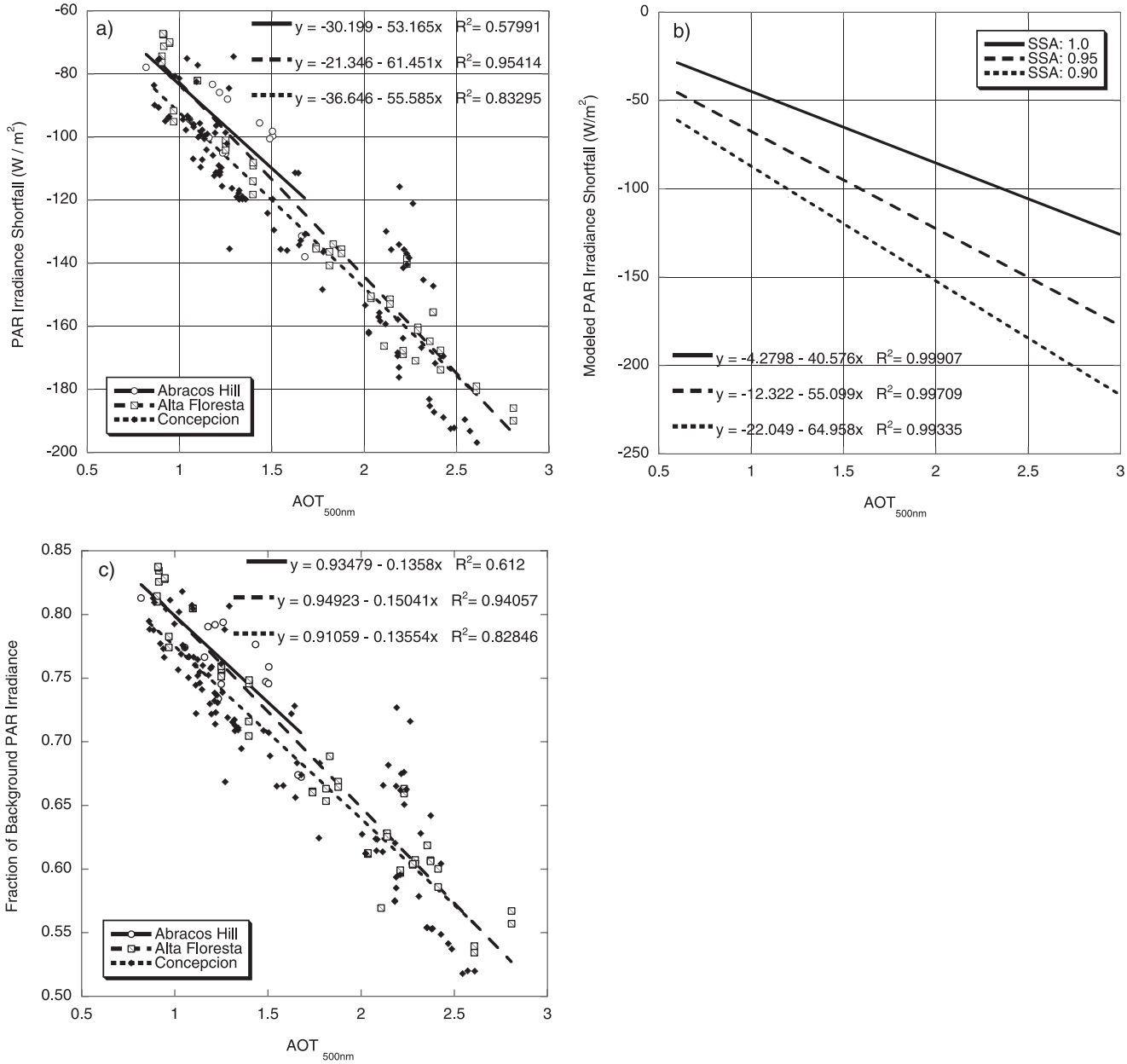

Figure 10. a) Computed PAR irradiance reductions from modeled PAR irradiance values for assumed cloud-free, background-aerosol conditions at 3 sites during 1998 (Concepcion) and 1999 (Alta Floresta, Abracos Hill) biomass burning intervals. b) 6S-modeled reductions in PAR irradiance for smoke aerosol with 3 different assumed single scattering albedo (SSA) values. c) Same as a) with the reductions expressed as fractional values.

region and generally compare well with CIMEL retrievals of this parameter from the same period (detailed in the section 3.4 below). Figure 10c displays the same data as in Figure 10a, with the reduction of PAR expressed as a fraction of modeled PAR flux for background conditions.

3.4. Single Scattering Albedo Estimation

[33] For CIMEL observations that were evaluated to be cloud-free by the AERONET cloud-screening algorithm, concurrent aerosol data from collocated CIMELs were used to investigate the optical properties of smoke aerosols. PAR flux data (1-minute sampling interval measurements) were matched with CIMEL observations acquired within ± 2 min. The CIMEL-derived atmospheric parameters of AOT, Angstrom wavelength exponent, and column water vapor were then associated with the nearly simultaneous PAR measurements and the data were filtered to reject cases with solar zenith angle greater than 40 degrees, $AOT_{440\ nm}$ less than 0.8 and wavelength exponent less than 1.0. The Angstrom wavelength exponent was computed as a linear regression of ln(AOT) vs. ln(wavelength) for the wavelengths (440,500,675 and 870 nm). This procedure was applied to the burning season data at Alta Floresta and Abracos Hill (1999) and Concepcion, Bolivia (1998). The final matched data sets of PAR and corresponding CIMEL measurements contained 48 obser-

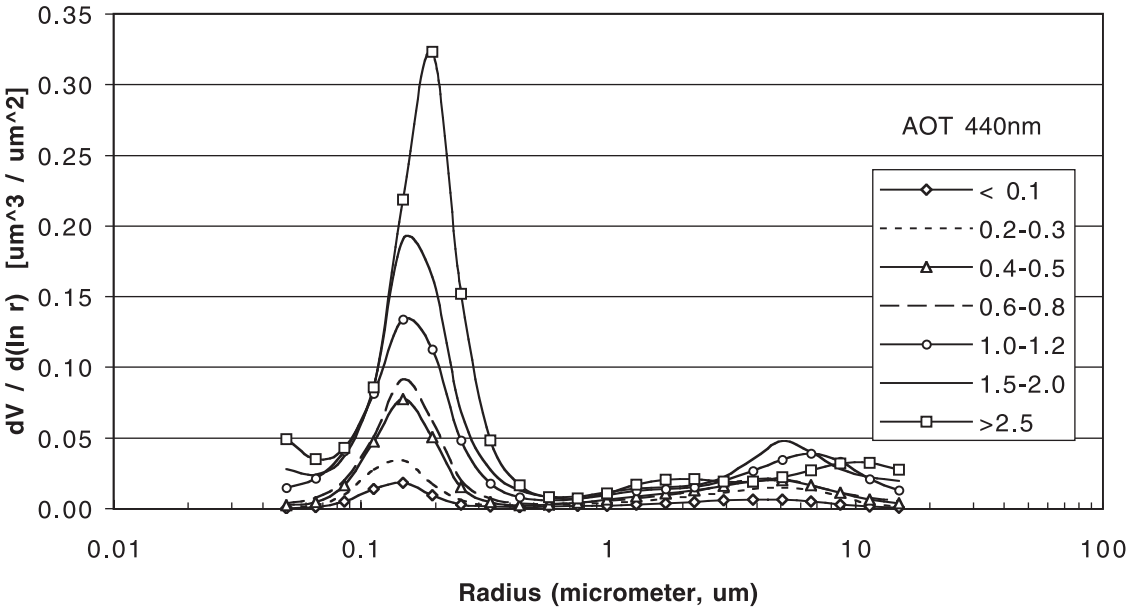

Figure 11. Aerosol volume size distributions averaged by AOT range for use in irradiance modeling procedures. Averages are based on the full record of volume size distribution retrievals derived from CIMEL radiance measurements at Abracos Hill in 1999.

vations for Alta Floresta (from 14 different days), 60 at Abracos Hill, and 183 at Concepcion.

[34] These data were used as input to the 6S model using the observed atmospheric properties during each flux measurement as well as the appropriate solar zenith angle and day of year. The aerosol size distribution was also an input parameter and was based on an average of distributions derived from the set of optimal CIMEL retrievals during year of 1999 at Abracos Hill, Brazil (Figure 11). The size distributions were grouped into 15 bins according to AOT value, and the appropriate size distribution was automatically utilized in 6S based on the given AOT. Based on each set of observed properties, the expected flux was modeled for a range of imaginary refractive indices (n_i) 0.000 to 0.061, to determine the trend of PAR flux for increasingly absorbing aerosols. These refractive indices represent a range of single scattering albedo (SSA) of approximately 0.75 to 1.0. A trendline was fitted to the resultant modeled fluxes and assumed SSA, and then the measured PAR flux was used to interpolate the theoretical SSA for each observation. The SSA estimates acquired are assumed to effectively represent the absorption properties at approximately 550nm, which is the central wavelength of the PAR sensor response curve (400–700 nm).

[35] The basic principles of this technique are identical to those employed by Eck et al. in similar studies in Brazil and Africa [*Eck et al.*, 1998, 2000], though the implementation has been modified.

[36] The single scattering albedos retrieved using the PAR measurements were generally similar at the 3 sites, perhaps due to the common nature of the biomass source (forest) and the prevalent wind patterns of the season that routinely transports smoke great distances in a westerly direction along the site transect. Since many of the retrieved SSA are often derived from a single day, statistics for daily average values were also compiled. The number of days with at least one SSA estimate was 17 at Alta Floresta, 9 at Abracos Hill, and 16 at Concepcion. Based on these daily averages, the median SSA for the sites were between 0.89 and 0.91 with a standard deviation of 0.03 or less. Considering all the individual retrievals, the estimates of SSA at all locations ranged from a minimum of 0.86–0.87 to a maximum of 0.93–0.96 (Table 1). The typical standard deviation of SSA for an individual day was less than 0.01.

[37] The CIMEL sunphotometer radiance measurements are also operationally processed with a new inversion code [*Dubovik et al.*, 1998, 2000; *Dubovik and King*, 2000] to

Table 1. Statistics of SSA Estimates From PAR Flux Measurements and CIMEL Sky Radiance Inversions for Three Sites[a]

	Alta Floresta (1999)	Abracos Hill (1999)	Conception (1998)
From PAR: Median (day average)	0.91	0.90	0.89
St Dev (day average)	0.02	0.03	0.03
Minimum (all points)	0.87	0.87	0.86
Maximum (all points)	0.95	0.96	0.93
From Cimel: Median (day average)	0.93	0.93	0.93
St Dev (day average)	0.02	0.01	0.02

[a] Statistics are based on daily averages of SSA estimates evaluated for Concepcion (1998), Alta Floresta (1999), and Abracos Hill (1999).

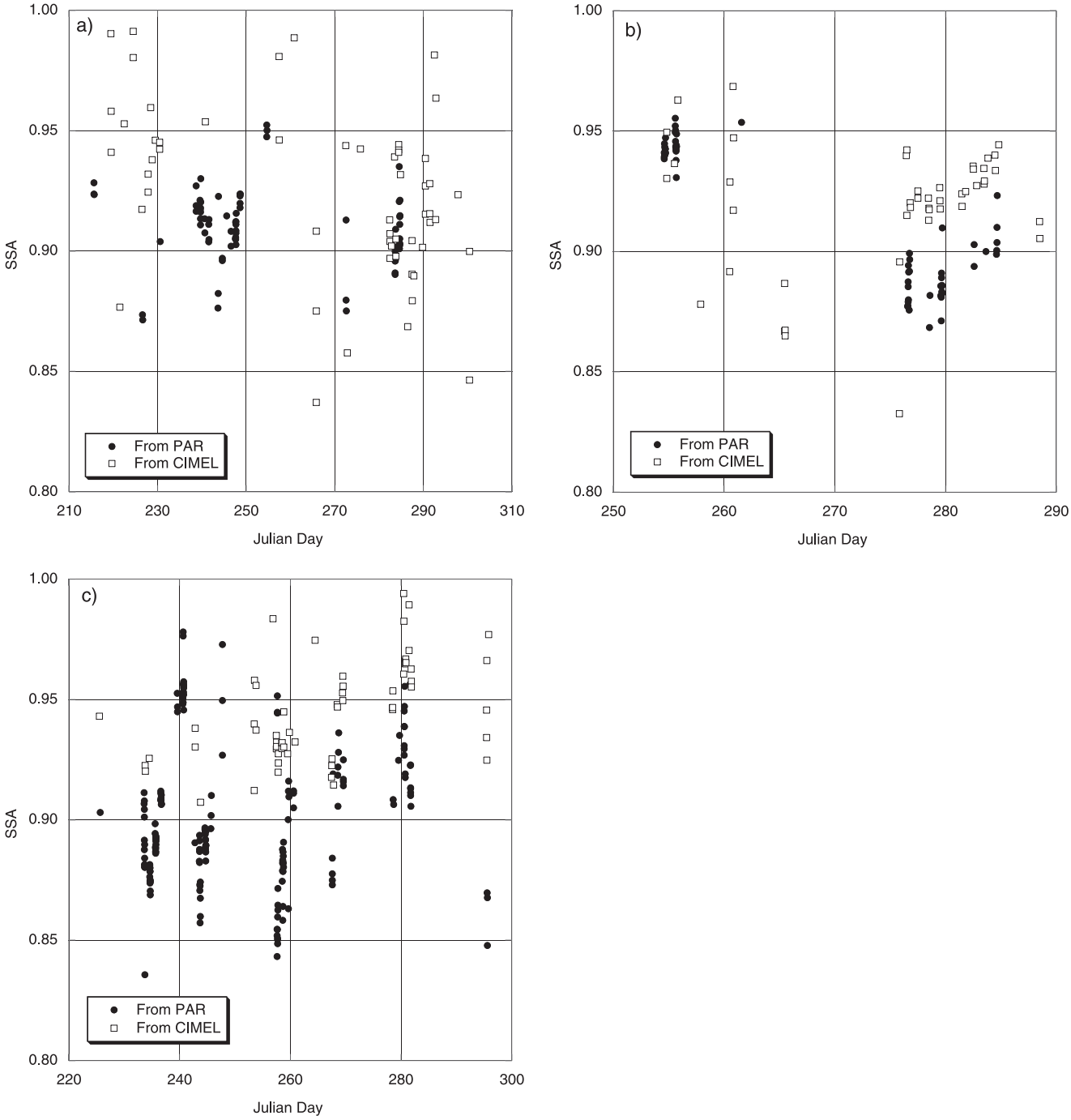

Figure 12. a) Single scattering albedo (SSA) estimates based on PAR flux measurements and CIMEL sky radiance inversions at Alta Floresta in 1999. Qualifying data are restricted to those satisfying AOT, solar zenith and retrieval error constraints described in the text. b) Same as a) for Abracos Hill data from 1999. c) Same as a) for Concepcion data from 1998.

produce estimates of SSA at four wavelengths (440 nm, 500 nm, 670 nm and 870 nm). The radiance inversion technique is most accurate when $AOT_{440\ nm}$ is greater than 0.4, solar zenith angle is larger than 45°, and the sky-radiance fitting error is less than 5%. Therefore, CIMEL-derived SSA products used in this study were restricted to those that met the above criteria.

[38] SSA estimates derived from the PAR flux method were found to consistently provide values lower than the sky radiance by an average of 0.03 (Figure 12). This discrepancy is within the expected uncertainty of the methods, estimated at 0.03 for both the sky radiance method and the PAR flux method. A number of known factors could produce differences. These include:

1. Non-simultaneity of observations: PAR-derived retrievals were all acquired for solar zenith angle <40° while those derived from sky radiance measurements were all restricted to solar zenith angle >45°

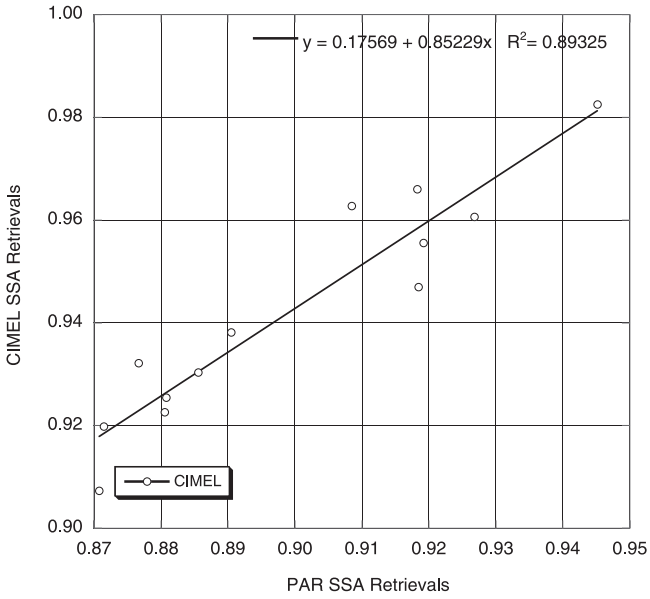

Figure 13. a) Correlation of single scattering albedo (SSA) estimates derived with PAR flux measurements and CIMEL sky radiance inversions. Data compared are estimates based on observations acquired within the same 1.5 hour interval.

2. Absolute calibration of sensors: PAR accuracy (± 3%); sky radiance accuracy (5%). The importance of absolute PAR calibrations is diminished by calibrating the sensors versus the same radiative transfer model used for this procedure.

3. Non-uniformity of smoke: When variable smoke plumes are present, the AOT observed by the CIMEL may not be representative of the full sky conditions to which the flux sensors are sensitive.

4. Cloud contamination: The cloud-screening algorithm applied to the CIMEL measurements only ensures a cloud-free circumsolar region. PAR measurements associated with these observations may potentially be affected by peripheral clouds. This is less of a problem than it could be given the general suppression of clouds during heavy burning conditions.

5. Cosine errors: Although the PAR measurements were restricted to solar zenith <40° (where cosine errors are minimal), as AOT increases, the incident hemispherical flux upon the sensor becomes more isotropic. This, in turn, increases the relative contribution of flux at low incidence angles that are characterized by poor cosine response, and may lead to an underestimation of the irradiance.

[39] The last of these points may be the most plausible for the possible negative bias to the SSA estimates derived from PAR measurements. If the flux is underestimated, it creates an appearance of additional absorption that is manifested as a lower SSA. Contrary to this hypothesis, however, no trend with AOT is evident in the discrepancy between the sky radiance and flux method. In fact, the correlation between the derived products of the two methods is quite strong, both for daily average SSA values and for retrievals that are relatively coincident in time. While the different solar geometry restrictions preclude simultaneous retrievals of the two methods, the Concepcion site had 15 cases when each type of retrieval was acquired within a 1.5 hour span. For this set of data, the correlation coefficient was 0.95, indicating that the two techniques were similarly responsive to the absorption properties of the aerosol (Figure 13). Even for the comparison of daily average SSA estimates there was strong correlation (0.76), although the retrievals by each technique may have been obtained many hours apart.

4. Conclusion

[40] This study has focused on characterizing the substantial influence of clouds and aerosols on the solar energy reaching the ground on a year-round basis. The effects of smoke aerosol alone during the heaviest months of biomass burning have been observed to produce reductions in insolation comparable to those resulting from persistent cloud cover in the latter phase of the wet season. Instantaneous reductions of PAR irradiance from the values expected for background (preburning) aerosol conditions are shown to average 86 W m^{-2} for smoke aerosol optical depths of 1.0, with reductions of ~55 W m^{-2} indicated for a unit change of AOT. Since smoke aerosol optical depths routinely average greater than 1.0 for several months of the year, the implications for vegetation productivity warrant further investigation.

[41] Modification of the spectral signal of incoming solar radiation during smoke intervals was examined as manifested in changes to the PAR fraction. Smoke aerosol was found to be the prominent factor causing variability in this parameter, at times lowering the ratio by more than 0.1 from typical, preburning values, indicating a disproportionate reduction of PAR relative to the full solar spectrum. This has consequences for researchers who may estimate PAR or total solar insolation by applying an fixed PAR fraction assumption to predict one flux from the other. For a common approximation of PAR as comprising 50% of the total solar signal, this could produce errors of 10% or more in derived flux during long periods within the dry season.

[42] The effect of water vapor upon PAR fraction was also found to have a definite, albeit minor influence which should not be ignored. Notably, the modification of this ratio by the presence of clouds was not observed to be significant based on the indicators of cloud presence used in this study. However, the clouds were observed to produce frequent, often large increases in the irradiance measurements above expected clear sky values. The PAR flux data for a five month period at one site revealed that enhancements of PAR irradiance of 10% or greater occurred in 24% of the measurements due to reflections from vertically developed cloud edges.

[43] The single scattering albedo (SSA) of dry season smoke aerosol was also estimated using PAR irradiance measurements and the 6S radiative transfer code, as well as with CIMEL sunphotometer sky radiance inversions. Comparison of the two techniques at 3 sites revealed a discrepancy with SSA values determined from PAR fluxes (daily average SSA: 0.89–0.91) uniformly lower than those derived from the CIMEL sunphotometer (0.93), although the correlation of the two methods was quite strong (R^2: 0.89).

[44] **Acknowledgments.** We thank the site managers responsible for maintaining the instrumentation suites and ensuring continuous, high quality data sets. These colleagues include Edilson Bernardino de Andrade

(Alta Floresta), Rosivaldo Lelis da Silva and Fabricio Berton Zanchi (Abracos Hill), Evan Everton (Belterra) and Zairon (Balbina).

[45] P. Artaxo acknowledges financial support from FAPESP.

References

Aber, J. D., and R. Freuder, Variation among solar radiation data sets for the eastern US and its effects on predictions of forest production and water yield, *Clim. Res.*, *15*(1), 33–43, 2000.

Ackerman, A. S., O. B. Toon, D. E. Stevens, A. J. Heymsfield, V. Ramanathan, and E. J. Welton, Reduction of tropical cloudiness by soot, *Science*, *288*, 1042–1047, 2000.

Balasubramanian, R., T. Victor, and R. Begum, Impact of biomass burning on rainwater acidity and composition in Singapore, *J. Geophys. Res.*, *104*(D21), 26,881–26,890, 1999.

Blackburn, W. J., and J. T. A. Proctor, Estimating photosynthetically active radiation from measured solar irradiance, *Sol. Energy*, *31*(2), 233–234, 1983.

Charlson, R. J., Direct climate forcing by anthropogenic sulfate aerosols: The Arrhenius paradigm a century later, *Ambio*, *26*(1), 25–31, 1997.

Charlson, R. J., and J. Heintzenberg, in *Aerosol Forcing of Climate*, edited by R. J. Charlson and J. Heintzenberg, chap. 1, pp. 1–10, John Wiley, New York, 1995.

Davies, S. J., and L. Unam, Smoke-haze from the 1997 Indonesian forest fires: Effects on pollution levels, local climate, atmospheric CO_2 concentrations, and tree photosynthesis, *For. Ecol. Manage.*, *124*(2–3), 137–144, 1999.

Dubovik, O., and M. D. King, A flexible inversion algorithm for retrieval of aerosol optical properties from Sun and sky radiance measurements, *J. Geophys. Res.*, *105*(D16), 20,673–20,696, 2000.

Dubovik, O., B. N. Holben, Y. J. Kaufman, M. Yamasoe, A. Smirnov, D. Tanre, and I. Slutsker, Single-scattering albedo of smoke retrieved from the sky radiance and solar transmittance measured from ground, *J. Geophys. Res.*, *103*(D24), 31,903–31,923, 1998.

Dubovik, O., A. Smirnov, B. N. Holben, M. D. King, Y. J. Kaufman, T. F. Eck, and I. Slutsker, Accuracy assessements of aerosol optical properties retrieved from Aerosol Robotic Network (AERONET) sun and sky radiance measurements, *J. Geophys. Res.*, *105*(D8), 9791–9806, 2000.

Eck, T. F., B. N. Holben, I. Slutsker, and A. Setzer, Measurements of irradiance attenuation and estimation of aerosol single scattering albedo for biomass burning aerosols in Amazonia, *J. Geophys. Res.*, *103*(D24), 31,865–31,878, 1998.

Eck, T. F., et al., Characterization of the optical properties of biomass burning aerosols in Zambia during the 1997 ZIBBEE experiment, *J. Geophys. Res.*, in press, 2000.

Facchini, M. C., M. Mircea, S. Fuzzi, and R. J. Charlson, Cloud albedo enhancement by surface-active organic solutes in growing droplets, *Nature*, *401*(6750), 257–259, 1999.

Frouin, R., and R. T. Pinker, Estimating photosynthetically active radiation (PAR) at the Earth's surface from satellite observations, *Remote Sens. Environ.*, *51*, 98–107, 1995.

Hansen, J., M. Sato, and R. Ruedy, Radiative forcing and climate response, *J. Geophys. Res.*, *102*, 6831–6864, 1997.

Holben, B. N., A. Setzer, T. F. Eck, A. Pereira, and I. Slutsker, Effect of dry-season biomass burning on Amazon basin aerosol concentrations and optical properties, 1992–1994, *J. Geophys. Res.*, *101*(D14), 19,465–19,481, 1996.

Holben, B. N., et al., AERONET—A federated instrument network and data archive for aerosol characterization, *Remote Sens. Environ.*, *66*, 1–16, 1998.

Konzelmann, T., D. R. Cahoon, and C. H. Whitlock, Impact of biomass burning in equatorial Africa on the downward surface shortwave irradiance: Observations versus calculations, *J. Geophys. Res.*, *104*(D17), 22,833–22,844, 1996.

Lawlor, D. W., Photosynthesis, productivity and environment, *J. Exp. Bot.*, *46*, 1449–1461, 1995.

Mims, F. M., B. N. Holben, T. F. Eck, B. C. Montgomery, and W. B. Grant, Smoky skies, mosquitoes, and disease, *Science*, *276*(5320), 1774–1775, 1997.

Monteith, J. L., and J. Elston, Climatic constraints on crop production, in *Plant Adaptation to Environmental Stress*, chap. 1, pp. 3–17, Chapman and Hall, New York, 1993.

Papaioannou, G., N. Papanikolaou, and D. Retalis, Relationships of photosynthetically active radiation and shortwave irradiance, *Theor. Appl. Climatol.*, *48*, 23–27, 1993.

Papaioannou, G., G. Nikolidakis, D. Asimakopoulos, and D. Retalis, Photosynthetically active radiation in Athens, *Agric. For. Meteorol.*, *81*, 287–298, 1996.

Pereira, E. B., F. R. Martins, and S. L. Abreu, Biomass burning controlled modulation of the solar radiation in Brazil, *Adv. Space Res.*, *24*(7), 971–975, 1999.

Pinker, R. T., and I. Laszlo, Global distribution of photosynthetically active radiation as observed from satellites, *J. Clim.*, *5*(1), 56–65, 1992.

Radojevik, M., and K. S. Tan, Impacts of biomass burning and regional haze on the pH of rainwater in Brunei Darussalam, *Atmos. Environ.*, *34*(17), 2739–2744, 2000.

Rao, C. R. N., Photosynthetically active components of global solar radiation: Measurements and model computations, *Arch. Meteorol. Geophys. Bioklimatol., Ser. B*, *34*, 353–364, 1984.

Rodskjer, N., Spectral daily insolation at Uppsala, Sweden, *Arch. Meteorol. Geophys. Bioklimatol., Ser. B*, *33*, 89–98, 1983.

Rosenfeld, D., TRMM observed first direct evidence of smoke from forest fires inhibiting rainfall, *Geophys. Res. Lett.*, *26*(20), 3105–3108, 1999.

Rosenfeld, D., Suppression of rain and snow by urban and industrial air pollution, *Science*, *287*(5459), 1793–1796, 2000.

Schwartz, S. E., et al., Connections between aerosol properties and climate forcing, in *Aerosol Forcing of Climate*, edited by R. J. Charlson and J. Heintzenberg, chap. 14, pp. 251–280, John Wiley, New York, 1995.

Smirnov, A., B. N. Holben, T. F. Eck, O. Dubovik, and I. Slutsker, Cloud-screening and quality control algorithms for the AERONET database, *Remote Sens. Environ.*, *73*(3), 337–349, 2000.

Suckling, P. W., J. A. Davies, and J. T. A. Proctor, The transmission of global and photosynthetically active radiation within a dwarf apple orchard, *Can. J. Bot.*, *53*, 1428–1441, 1975.

Toon, O. B., Modeling aerosol properties and climatic effects, in *Aerosol Forcing of Climate*, edited by R. J. Charlson and J. Heintzenberg, chap. 11, pp. 197–213, John Wiley, New York, 1995.

Vermote, E. F., D. Tanre, J. L. Deuze, M. Herman, and J. J. Morcrette, Second simulation of the satellite signal in the solar spectrum, 6S: An overview, *IEEE Trans. Geosci. Remote Sens.*, *35*, 675–686, 1997.

Wild, M., Discrepancies between model-calculated and observed shortwave atmospheric absorption in areas with high aerosol loadings, *J. Geophys. Res.*, *104*(D22), 27,361–27,371, 1999.

Zhang, X., Y. Zhang, and Y. Zhoub, Measuring and modeling photosynthetically active radiation in Tibet plateau during April–October, *Agric. For. Meteorol.*, *102*, 207–212, 2000.

J. S. Schafer, Science Systems and Applications, Inc. (SSAI), Lanham, MD 20706, USA. (jschafer@aeronet.gsfc.nasa.gov)

B. N. Holben, Biospheric Sciences Branch, Code 923, NASA/GSFC, Greenbelt, MD 20771, USA.

T. F. Eck, Goddard Earth Sciences and Technology Center, University of Maryland Baltimore County, Catonsville, MD, USA.

P. Artaxo and M. A. Yamasoe, Departamento de Física Aplicada, Instituto de Física, Universidade de São Paulo, Rua do Matão, Travessa R, 187, São Paulo, SP CEP 05508-900, Brazil.